The International Journal of Advanced Manufacturing Technology (2023) 125:5323–5343
https://doi.org/10.1007/s00170-023-10898-0

ORIGINAL ARTICLE

Using micro-milled surface topography and force measurements to identify tool runout and mechanistic model coefficients

Abdulrzak Masrani[1] · **Yiğit Karpat**[1,2,3]

Received: 16 September 2022 / Accepted: 12 January 2023 / Published online: 15 February 2023

Abstract
Modeling the forces during micro-milling processes is directly linked to the chip load and mechanistic model parameters that are generally dependent on the tool/work combination. Tool runout, deflection, and the material's elastic recovery mainly affect the chip load as a function of feed. Experimentally measured micro-milling forces can be employed to identify cutting force coefficients and runout parameters. However, decoupling the interplay among runout, deflection, and elastic recovery is difficult when only measured forces are considered. In this paper, machined surface topography has been considered as an additional process output to investigate the influence of runout and deflection separately. The machined surface topography was investigated using a scanning laser microscope to identify minimum chip thicknesss and runout parameters. A finite element model of tool deflection has been developed based on the end mill geometry used in the experiments. The finite element model was used to obtain a surrogate model of the tool deflection which was implemented into the mechanistic model. Nanoindentation tests were conducted on the coated WC tool to identify its material properties which are employed in the finite element model. An uncut chip thickness model is constructed by considering preceding trochoidal trajectories of the cutting edge, helix lag, tool runout, tool deflection, and the chip thickness accumulation phenomenon. The force model was validated experimentally by conducting both slot and side milling tests on commercially pure titanium (cp-Ti). The predicted cutting forces were shown to be in good agreement with the experimental cutting forces.

Keywords Micro-milling · Force modeling · Tool runout · Deflection · Surface topography

1 Introduction

A global miniaturization trend in manufacturing stimulates the need for small parts. Micro-milling can be used to manufacture parts of complex 3D geometry in a broad spectrum of materials with high accuracy and productivity [1–3]. The ability to predict process outputs is crucial to reducing manufacturing costs by eliminating the trial and error phase during process planning. Within the framework of smart manufacturing, it is essential to optimize the process parameters and monitoring the process outputs through predictive models based on process physics. Some crucial considerations such as tool runout, tool deflections, elastic recovery, and chip accumulation must be included in micro-milling force models to enhance their predictive ability.

Micro-end mills with diameters less than 1 mm are commonly used in micro-milling. As a result, feed is set low, which usually happens to be in the same order of magnitude as the edge radius of the tool. Chip formation is associated with a minimum uncut chip thickness, which is defined relative to the edge radius of the tool. When uncut chip thickness is less than this critical value, the tool mainly ploughs the workpiece material, and no cutting occurs [4, 5]. Liu et al. [6] developed a model for micro-milling where material properties and friction conditions were used to estimate the minimum chip thickness. Rezaei et al. [7] studied this issue for different materials and found that the minimum chip thickness to edge radius ratio changes between 25

✉ Yiğit Karpat
ykarpat@bilkent.edu.tr

Abdulrzak Masrani
a.masrani@bilkent.edu.tr

[1] Department of Mechanical Engineering, Bilkent University, Ankara, 06800, Turkey

[2] Department of Industrial Engineering, Bilkent University, Ankara, 06800, Turkey

[3] UNAM – Institute of Materials Science and Nanotechnology, Bilkent University, Ankara, 06800, Turkey

and 49%. The uncut work material increases the chip load in the following tool pass and hence affects the forces.

A general approach in micro-milling force modeling is to calculate the uncut chip thickness as a function of tool rotation angle. The effects of tool runout, chip accumulation, and tool deflection should also be considered. Manufacturing issues related to the spindle, micro-end mill, and tool holder contribute to the resulting runout. Runout is characterized by runout radius and angle parameters. Runout modeling is also essential to identify the entry and exit angles of the process. In a pioneering study, Bao and Tansel [8] showed the effect of runout on force fluctuations and tool wear. Li et al. [9] proposed a runout model to calculate three-dimensional cutting forces. Mamedov and Lazoglu [10] compared chip thickness models considering runout available in the literature for micro-milling based on force predictions. Afazov et al. [11] included the effect of helix lag in runout modeling in micro-milling, which improved force predictions. Another factor affecting entry and exit angles is the accumulation of uncut material, which occurs during the machining process due to the transition between ploughing and cutting [12]. Measurement of runout is not straightforward in micro-milling, especially under dynamic conditions. Advanced measurement systems are required to identify the runout parameters [13–15]. In an alternative approach, Attanasio [16] proposed an experimental methodology requiring measurements from micro-milled slots to identify runout parameters. Machining under conditions where feed and runout radius are close may rapidly lead to uneven wear on the cutting edges, which further increases the forces. The tool would deflect even more, resulting in tool breakage and geometric errors on the machined surfaces [17]. Tool deflection is included in the force models through analytical models where the complex helical tool geometry is simplified to a cylinder with an equivalent diameter [18, 19]. This approach allows fast calculation of the tool deflection for forces applied to the tool during cutting. Moges et al. [20] showed the influence of including tool deflections on the forces especially during micro-side milling.

The cutting edge radius, material properties, and the interaction between the tool and the work material play a significant role in elastic recovery. Elastic recovery affects the contact conditions on the flank face of the cutting edge. In addition, calculating the contact area on the flank face is essential in terms of the effect of ploughing forces, and it requires the elastic recovery rate to be known. Malekian et al. [21] and Zhang et al. [22] used scratching tests to identify the elastic recovery rate and used that information to calculate the volume of ploughed material under the tool.

Once the chip thickness is calculated, the most straightforward approach to obtain milling forces is using a mechanistic modeling approach, where experimentally measured process forces are used to identify cutting force coefficients [23]. The cutting force coefficients include the material's resistance to cut with all the above-mentioned effects. Another common approach is to use finite element simulation of the machining process based on thermo-physical material properties. The success of finite element simulation mainly depends on the definition of work material constitutive model friction conditions. Finite element simulation outputs in 2D machining have been used to replace the milling experiments to calculate the cutting force coefficients, as shown in [11, 24–27]. While 2D finite element models are preferred due to their faster computation time, Attanasio et al. [28] included the effect of tool runout in 3D finite element simulation of the micro-milling process and obtained acceptable results.

Tool runout, tool deflection, and elastic recovery all affect the topography of the micro-milled surfaces. Vogler et al. [29] modeled the centerline surface roughness in micro-milling considering the effects of tool geometry and minimum chip thickness. Krüger and Denkena [30] modeled the influence of runout on the surface roughness based on cutting forces. Mathematical models for predicting the surface generated on the slot floor during micro-milling, considering the effect of elastic recovery and tool runout, have been proposed in the literature [31, 32].

To accurately identify the micro-milling force model parameters, a comprehensive force model must include many of the associated phenomena. This study uses machined surface topography information together with micro-milling force measurements to identify the unknown parameters. The feed marks left by the cutting teeth on the machined surface have been investigated and incorporated into the uncut chip thickness model through an optimization algorithm. The uncut chip thickness model is extended to consider multiple previous trochoidal passes of the micro-end-mill teeth, which enhances the uncut chip thickness estimation accuracy near the entry and exit angles. Tool deflection and chip thickness accumulation are also considered in the developed model.

The structure of this paper will be as follows: the micro-milling force model is explained in Section 2. The experimental setup is presented in Section 3. In Section 4, the machined surface investigation is conducted. The cutting force coefficients are identified in Section 5. Finally, the results are presented in Section 6.

2 Micro-milling force model

A general overview of the model used in this study is presented in Fig. 1. The uncut chip thickness is calculated from the trochoidal tooth trajectory considering the accumulative tool and spindle system runout (Fig. 1a)

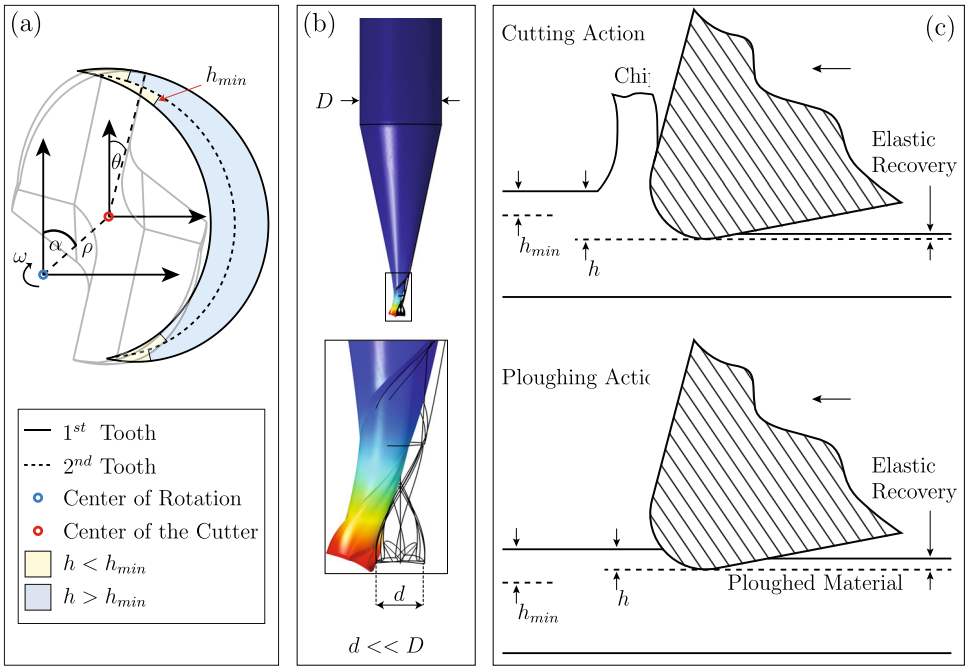

Fig. 1 Phenomena associated with micro-milling: (a) runout, (b) deflection, (c) chip accumulation due to ploughing action

and the helix lag. An initial value of the uncut chip thickness assuming a rigid tool is calculated from the trochoidal trajectory of the teeth considering runout. Tool deflection (Fig. 1b) through a finite element based model and chip thickness accumulation due to ploughing action (Fig. 1c) are also considered in the model. The details of the model are explained below.

The immersed depth of the micro-end mill is first discretized into K axial disc elements of equal thickness dz to accommodate helix lag β, as depicted in Fig. 2. For a micro-end mill with a number of cutting teeth of N_z, a radius of R, and a helix angle of λ, cutting at an axial depth of cut of a_p, the immersion angle of the jth cutting tooth at the ith disc element during the tool rotation $\theta_{i,j}$ is described in terms of time as Eq. 1:

$$\theta_{i,j} = \omega t_i - \frac{2\pi j}{N_z} \tag{1}$$

where ω is the spindle speed in rad/s, $j = 0, 1 \ldots N_z - 1$, $i = 1 \ldots K$, and t_i is the time at the first cutting tooth at the ith disc element which is described as follows:

$$t_i = t_B - \frac{i(t_A - t_B)}{K} \tag{2}$$

where t_A, t_B are the time values at nodes A, B respectively. Taking t_A as a known starting time t_o, t_B can be calculated from:

$$t_B = t_A - \frac{\beta}{\omega} \tag{3}$$

The angle β can be calculated as in:

$$\beta = \arccos\left(\frac{2R^2 - a_p^2 \tan^2 \lambda}{2R^2}\right) \tag{4}$$

In mechanistic modeling, cutting forces are directly linked to the chip load. Mechanistic force models can take several forms, amongst which linear and power law models are the most common. A power law model is adopted in this study to capture both cutting and ploughing action as a function of uncut chip thickness. Two different sets of cutting coefficients are used to model forces in the ploughing and cutting regions considering the minimum uncut chip thickness value $h_{\min}$ [21]. The cutting forces are calculated in the rotating reference plane of the tool based on the power law mechanistic model as in Eq. 5:

$$dF_t(\theta_{i,j}) = \begin{cases} K_{tc}.h_{rda}(\theta_{i,j})^{a_{tc}}.dz & h_{rda}(\theta_{i,j}) \geq h_{\min} \\ K_{tp}.h_{rda}(\theta_{i,j})^{a_{tp}}.dz & h_{rda}(\theta_{i,j}) < h_{\min} \end{cases} \tag{5a}$$

$$dF_n(\theta_{i,j}) = \begin{cases} K_{nc}.h_{rda}(\theta_{i,j})^{a_{nc}}.dz & h_{rda}(\theta_{i,j}) \geq h_{\min} \\ K_{np}.h_{rda}(\theta_{i,j})^{a_{np}}.dz & h_{rda}(\theta_{i,j}) < h_{\min} \end{cases} \tag{5b}$$

where $dF_n(\theta_{i,j}), dF_t(\theta_{i,j})$ are the elemental normal and tangential components of the cutting force acting on the tool, $K_{tc}, a_{tc}, K_{nc}, a_{nc}$ are the force coefficients in the cutting dominated region ($h_{rda}(\theta_{i,j}) \geq h_{\min}$), $K_{tp}, a_{tp}, K_{np}, a_{np}$ are the force coefficients in the ploughing dominated region ($h_{rda}\left(\theta_{i,j}\right) < h_{\min}$), and dz is the axial element thickness in mm which is equal to:

$$dz = \frac{a_p}{K} \tag{6}$$

where a_p is the axial depth of cut in mm.

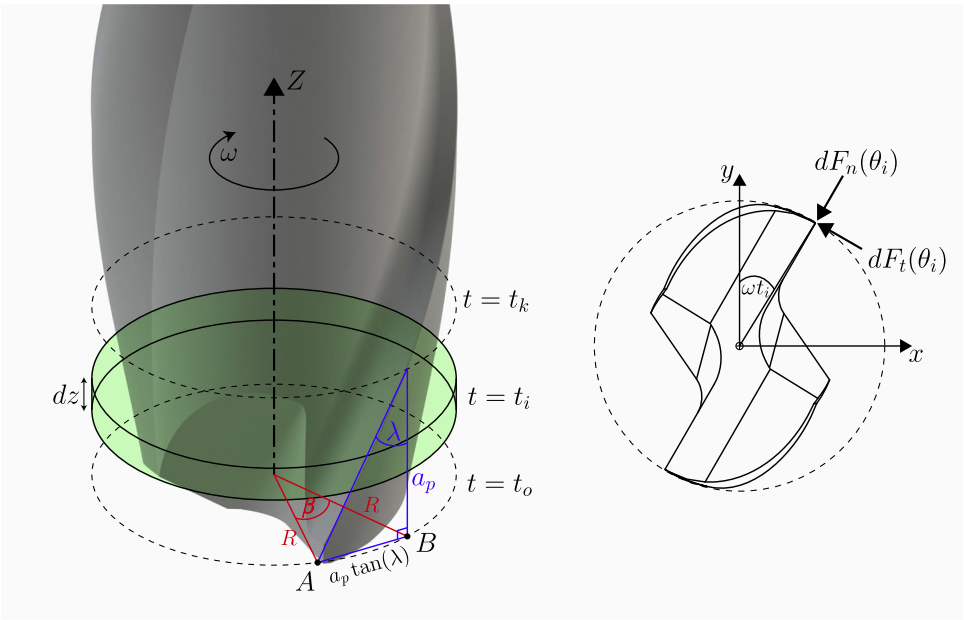

Fig. 2 Discretization of the engaged axial depth of the two-flute micro-end-mill

The cutting forces in the tool reference plane are calculated using Eq. 5 and then transformed into the reference plane of the workpiece using Eq. 7:

$$\begin{bmatrix} dF_x(\theta_{i,j}) \\ dF_y(\theta_{i,j}) \end{bmatrix} = \begin{bmatrix} -\cos(\theta_{i,j}) & -\sin(\theta_{i,j}) \\ \sin(\theta_{i,j}) & -\cos(\theta_{i,j}) \end{bmatrix} \begin{bmatrix} dF_t(\theta_{i,j}) \\ dF_n(\theta_{i,j}) \end{bmatrix} \tag{7}$$

The elemental cutting forces are then summed along the axial height of the tool to produce the final cutting force signal using Eq. 8.

$$F_{x,y}(t) = \sum_{i=1}^{K} \sum_{j=0}^{N_z-1} dF_{x,y}(\theta_{i,j}) \tag{8}$$

2.1 Runout model

The uncut chip thickness model considering runout is extended from the study of Afazov et al. [11]. A reference plane xoy is constructed on the workpiece as depicted in Fig. 3, such that the origin coincides with the tool center considering zero runout at the starting time t_o. For a micro-end-mill cutting at feed rates in the x, y directions as f_x, f_y (mm/min), having a runout of ρ (mm) and a runout angle of α radians, the trajectory of the center of the tool (denoted as C in Fig. 3) can be written as in Eq. 9.

$$x_C(t_i) = \frac{f_x t_i}{60} + \rho \sin(\omega t_i + \alpha) \tag{9a}$$

$$y_C(t_i) = \frac{f_y t_i}{60} + \rho \cos(\omega t_i + \alpha) \tag{9b}$$

The trajectory of the jth cutting tooth at the ith disc element at a specific instant in time t_i (point P) can be described with Eq. 10.

$$x_P(t_i) = x_C(t_i) + R \sin\left(\omega t_i - \frac{2\pi j}{N_z}\right) \tag{10a}$$

$$y_P(t_i) = y_C(t_i) + R \cos\left(\omega t_i - \frac{2\pi j}{N_z}\right) \tag{10b}$$

In a similar manner, points C', Q which correspond to the tool center and the previous cutting tooth trajectories, respectively, at a previous instant in time t_i' when the previous cutting tooth trajectory intersects the line CP can

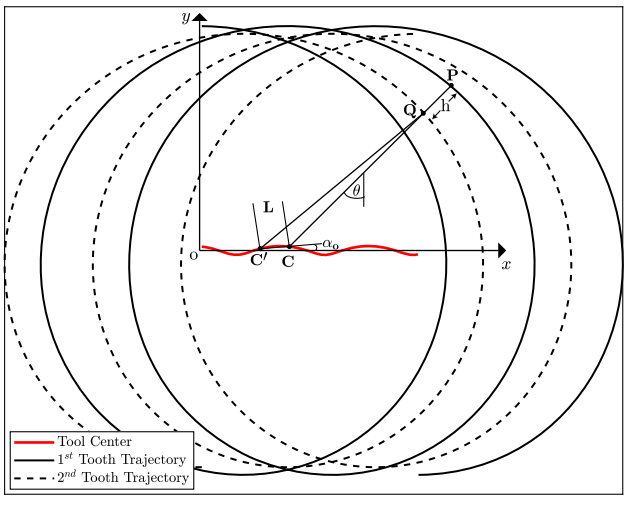

Fig. 3 Simulated trajectory of the cutting teeth of a two-flute ($N_z = 2$) micro-end-mill

be located by substituting t_i with t_i' and j with $j-1$ in Eqs. 9 and 10 as follows:

$$x_{C'}(t_i') = \frac{f_x t_i'}{60} + \rho \sin\left(\omega t_i' + \alpha\right) \tag{11a}$$

$$y_{C'}(t_i') = \frac{f_y t_i'}{60} + \rho \cos\left(\omega t_i' + \alpha\right) \tag{11b}$$

$$x_Q(t_i') = x_{C'}(t_i') + R \sin\left(\omega t_i' - \frac{2\pi(j-1)}{N_z}\right) \tag{12a}$$

$$y_Q(t_i') = y_{C'}(t_i') + R \cos\left(\omega t_i' - \frac{2\pi(j-1)}{N_z}\right) \tag{12b}$$

The time t_i' can be determined from the following geometric relation:

$$[x_P(t_i) - x_Q(t_i')] - [y_p(t_i) - y_Q(t_i')]\tan(\omega t_i) = 0 \tag{13}$$

Equation 14 can be written by substituting Eqs. 10 and 12 in Eq. 13 as follows:

$$\begin{aligned}
&\left\{\left[\frac{f_x t_i}{60} + \rho \sin\left(\omega t_i + \alpha\right) + R \sin\left(\omega t_i - \frac{2\pi j}{N_z}\right)\right]\right. \\
&\left.-\left[\frac{f_x t_i'}{60} + \rho \sin\left(\omega t_i' + \alpha\right) + R \sin\left(\omega t_i' - \frac{2\pi(j-1)}{N_z}\right)\right]\right\} \\
&-\left\{\left[\frac{f_y t_i}{60} + \rho \cos\left(\omega t_i + \alpha\right) + R \cos\left(\omega t_i - \frac{2\pi j}{N_z}\right)\right]\right. \\
&\left.-\left[\frac{f_y t_i'}{60} + \rho \cos\left(\omega t_i' + \alpha\right) + R \cos\left(\omega t_i' - \frac{2\pi(j-1)}{N_z}\right)\right]\right\} \tan(\omega t_i) = 0
\end{aligned} \tag{14}$$

Equation 14 can be solved for t_i' numerically using Newton-Raphson's method [33]. The initial guess can be written as follows:

$$t_{i\,o}' = t_i - \frac{2\pi}{\omega N_z} \tag{15}$$

After the value of t_i' is found, the uncut chip thickness considering runout and a rigid tool can be found from the geometric relation:

$$h_r(\theta_{i,j}) = R + L\sin(\theta_{i,j} + \alpha_o) - \sqrt{R^2 - L^2\cos^2(\theta_{i,j} + \alpha_o)} \tag{16}$$

The length L and the angle α_o can be calculated as follows:

$$L = \sqrt{\left[x_C(t_i) - x_{C'}(t_i')\right]^2 + \left[y_C(t_i) - y_{C'}(t_i')\right]^2} \tag{17}$$

$$\alpha_o = \arctan\left(\frac{y_C(t_i) - y_{C'}(t_i')}{x_C(t_i) - x_{C'}(t_i')}\right) \tag{18}$$

When the feed per tooth f_t is small in the presence of a relatively large runout, a jth cutting tooth can cut material left from not only the $(j-1)$th tooth pass, but several previous tooth passes. To illustrate, Fig. 4 presents the simulated cutting tooth trajectories at the first disc element $i = 1$ for a 2-flute micro-end mill. The figure presents two cases where the runout angle is held constant at 30°, and the runout and the feed per tooth values are changed. It can be observed that as the feed decreases, the effect of runout becomes more prominent, and the chip load varies significantly from one cutting tooth to another. In the case of slot milling with a 2-flute micro-end mill, this situation is visible at immersion angles closer to the cutter's entry and exit angles (the area highlighted in yellow in Fig. 4a). When the ratio f_t/ρ is in the vicinity of the number of teeth N_z, the second cutting tooth might not engage in the cut (Fig. 4b). In the case where the runout angle α is equal to zero and $f_t/\rho \leq N_z$, this situation becomes critical under the assumption of a rigid cutter. Therefore, to produce an accurate estimate of the uncut chip thickness at low feed rates and a large runout, it is necessary to consider not only one previous tooth pass but N_z number of the previous tooth passes. Equations 11–18 can be modified to produce a number of solutions for the uncut chip thickness $h_{r,n_j}(\theta_{i,j})$ that is equal to the number of flutes N_z of the micro-end-mill, essentially by substituting t_i' with t_{i,n_j} (denoting the time at the $(j-n_j)$th tooth pass), and $(j-1)$ with $(j-n_j)$, for $n_j = 1 \ldots N_z$. The initial guess for the Newton-Raphson method can then be modified to:

$$t_{i,n_j\,o} = t_i - \frac{2\pi n_j}{\omega N_z} \tag{19}$$

And the final estimate of the uncut chip thickness considering runout can be taken as the minimum of all the solutions as in Eq. 20.

$$h_r(\theta_{i,j}) = \min_{n_j=1\ldots N_z}\left(h_{r,n_j}\left(\theta_{i,j}\right)\right) \tag{20}$$

2.2 Tool deflection model

In micro-milling, tool deflection can significantly affect the tool-workpiece engagement and chip load, leading to geometric errors on the machined component. With

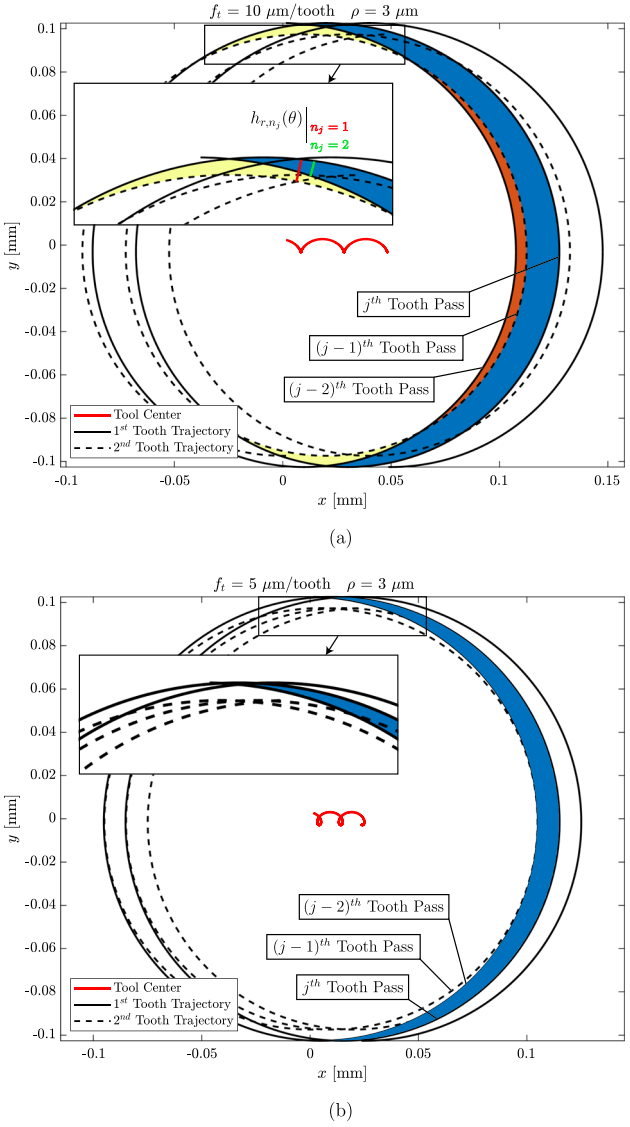

Fig. 4 Simulated cutting tooth trajectories in two different cases: (a) f_t = 10 μm/tooth , ρ = 3 μm. (b) f_t = 5 μm/tooth , ρ = 3 μm

decreasing tool diameter, deflections due to cutting forces cannot be omitted from the modeling process. While both the normal and tangential components of the cutting force contribute to the total deflection of the cutter during machining, deflection in the tangential direction has little effect on the uncut chip thickness. Therefore, static cutter deflection resulting from only the normal force component is considered in this work. Figure 5 shows the effect of cutter deflection on the formulation of the uncut chip thickness. A Hookean spring model can be applied to incorporate the effect of cutter deflection on the uncut chip thickness. For known tool stiffness k_n (N/mm), the following force balance equation can be written [25]:

$$F_n(\theta) = k_n.\delta h(\theta) \tag{21}$$

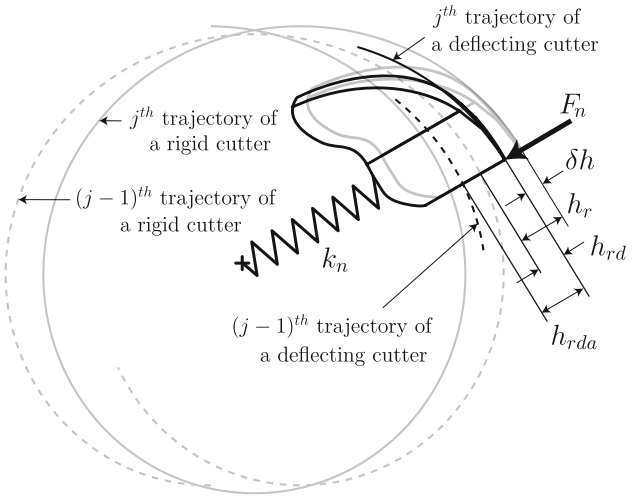

Fig. 5 Illustration of the influence of micro-end-mill deflection on the chip thickness

where $\delta h(\theta)$ is the cutter deflection in (mm). Equation 21 can be rewritten to describe the elemental normal force and deflection at the disc element level as in Eq. 22.

$$K_{nc}.h_{rd}\left(\theta_{i,j}\right)^{a_{nc}}.dz = \frac{k_n}{K}\left[h_r\left(\theta_{i,j}\right) - h_{rd}\left(\theta_{i,j}\right)\right] \tag{22}$$

Equation 22 is solved for $h_{rd}(\theta_i)$, which is the value of the uncut chip thickness with consideration of runout and deflection. The value of the cutter deflection δh is then calculated and added to the uncut chip thickness value in the $(j+1)$th tooth pass as in Eq. 24.

$$\delta h\left(\theta_{i,j}\right) = h_r\left(\theta_{i,j}\right) - h_{rd}\left(\theta_{i,j}\right) \tag{23}$$

$$h_{rd}\left(\theta_{i,j+1}\right) = h_{rd}\left(\theta_{i,j}\right) + \delta h\left(\theta_{i,j}\right) \tag{24}$$

In order to identify the value of the tool tip stiffness k_n, finite element analysis is carried out to investigate the tool tip deflection behavior under static load. The influence of runout parameters ρ, α together with tool deflection would be observed from the feed marks of the machined surface. The machined surface will be scanned using a laser scanning microscope, and analyzed as shown in Fig. 6. The information obtained from the machined surface topography will be utilized to solve Eq. 22 which is also dependent on normal direction force coefficient K_{nc}.

2.2.1 Finite element analysis of tool deflection

In order to predict tool deflection, an accurate estimation of the tool tip stiffness k_n in the normal direction is required. Studies have resolved to analytical modeling of the tool tip deflection, where the helical part of the tool tip is represented with an equivalent diameter [34]. Others have used experimental tests [25] to estimate the value of the tool tip stiffness. During these tests, the tool is clamped, and

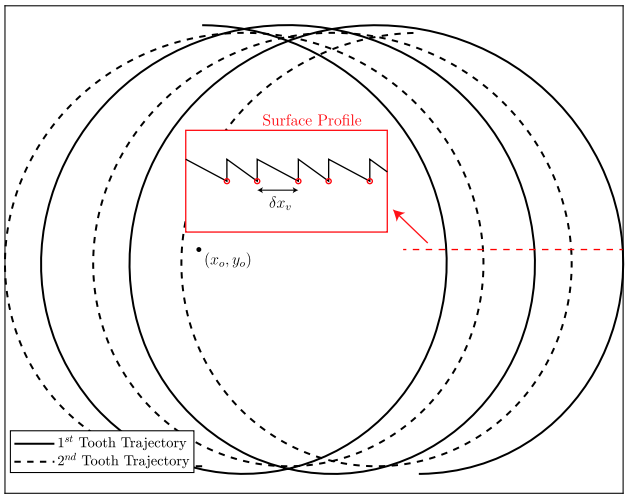

Fig. 6 Influence of tool runout and deflection on the centerline surface topography

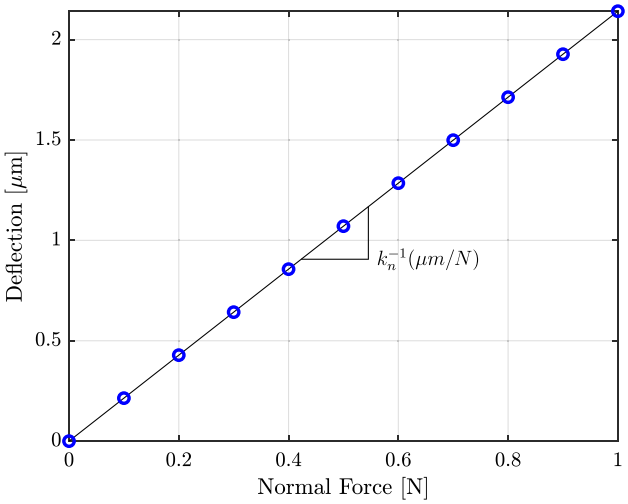

Fig. 8 Finite element simulation result

a variable load is applied to the tool tip while monitoring the tool tip deflection. In most cases, the machining center stage was used as a reference to measure the tool tip deflection, which is prone to errors bound by the accuracy of the stage. Moreover, applying the load precisely in the normal direction to the tool's cutting edge is not guaranteed experimentally considering the small diameters of the micro end mills. Finite element analysis (FEA) can be used to simulate such tests to obtain the tool tip stiffness. FEA allows for the accommodation of the complex geometry of micro-end mills and the accurate application of the load precisely in the normal direction over the rounded cutting edge of the tool. The tool design parameters such as the diameter, helix angle, cutting length, and number of teeth can be easily modified in the CAD model. The CAD model of the tool can then be transferred to FEA software to analyze the tool tip deflection, given that tool material properties are correctly defined. In this study, the tool geometry was inspected under a laser scanning microscope (VK-X100, Keyence, Japan), and a precise CAD model was developed using Solidworks CAD package (Dassault Systèmes, France). The CAD model was then imported to the COMSOL Multiphysics FE package (COMSOL Inc. USA) for the finite element analysis of tool deflection.

The amount of deflection depends on the modulus of elasticity of the tool material. Since the modulus of elasticity of the tool material may not be known exactly, a series of nanoindentation tests were carried out on the tool shank. Those tests were carried out in compliance with the ISO-14577 Nanoindentation Standard, and the modulus of elasticity of the tool material was measured to be 615.5 GPa. A quasi-static analysis was used in FE model, and a linear elastic material was applied to the tool geometry using the identified modulus of elasticity and a Poisson's ratio of 0.22. A tetrahedral mesh (Fig. 7a) was applied to the geometry

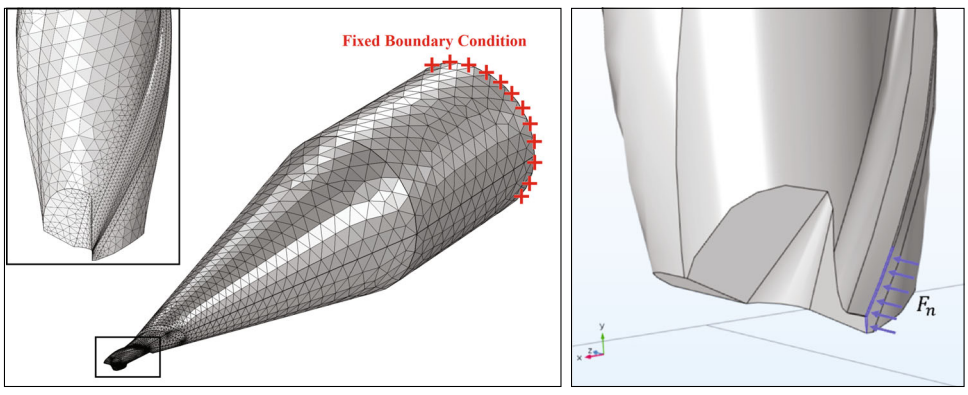

Fig. 7 Finite element simulation. (a) Finite element mesh and the fixed boundary condition. (b) Boundary load

with minimum and maximum element sizes of 10 and 500 μm, respectively, a maximum element growth rate of 1.35, and a curvature factor of 0.3. The mesh was optimized to produce consistent results with acceptable computational speed. A fixed boundary condition was applied at 15 mm from the tool tip, as depicted in Fig. 7a, which was the same overhang value used during the experimental cutting tests. The boundary load was applied to the rounded cutting edge of the tool in the normal direction, as depicted in Fig. 7b, in steps of 0.1 N using the parametric sweep feature of the software. The force was applied in the normal direction. The deflection of the tool center was recorded at every step during the parametric sweep, and the results are presented in Fig. 8. Linear regression was applied to the data points to produce a value of the tool tip stiffness in the normal direction k_n, which was found to be 0.47 N/μm.

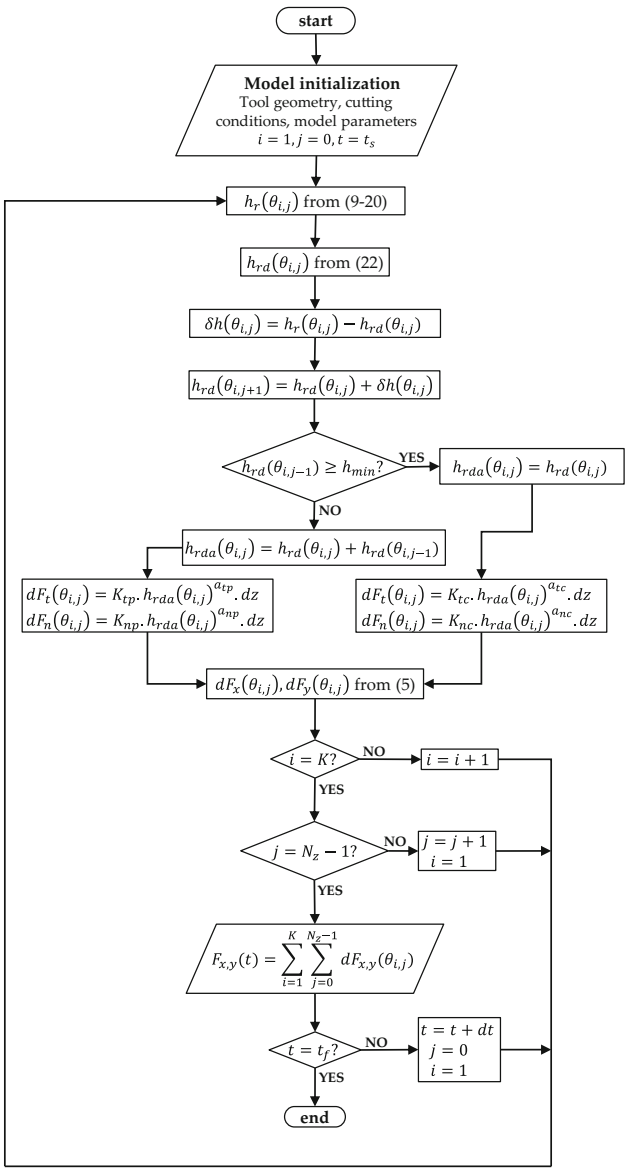

Fig. 9 Flow chart of the force model

2.3 Chip thickness accumulation

When the uncut chip thickness from the previous tooth pass is less than the minimum uncut chip thickness value, chip accumulation occurs, and the value of the uncut chip thickness at the current tooth pass h_{rd} is updated to h_{rda}. Therefore, the influences of the uncut chip thickness with consideration of runout, deflection, and chip thickness accumulation are included as shown in Eq. 25:

$$h_{rda}(\theta_{i,j}) = \begin{cases} h_{rd}(\theta_{i,j}) & h_{rd}(\theta_{i,j-1}) \geq h_{\min} \\ h_{rd}(\theta_{i,j}) + h_{rd}(\theta_{i,j-1}) & h_{rd}(\theta_{i,j-1}) < h_{\min} \end{cases} \tag{25}$$

The uncut chip thickness will continue to accumulate in the subsequent tooth passes until exceeding the minimum uncut chip thickness value [25]. The identification of the minimum uncut chip thickness will be performed on the machined surface topograhy, as discussed in Section 4.2.

A flow chart summarizing the force model for known runout parameters and cutting force coefficients is presented in Fig. 9. First, the model is initialized by defining the cutting conditions and tool parameters. An initial value of the uncut chip thickness is then calculated from Eqs. 9−20. The uncut chip thickness is then updated to accommodate tool deflection using Eq. 22. The amount of tool deflection is then accommodated in the subsequent tooth pass using Eqs. 23 and 24. The resulting uncut chip thickness for one preceding tooth pass is then compared with the minimum uncut chip thickness value, and the final estimate of the uncut chip thickness is then calculated from Eq. 25. The elemental cutting forces are then calculated in the rotating reference plane of the tool based on the mechanistic force model as shown in Eq. 5. The cutting forces in the fixed reference plane of the workpiece are then calculated and summed along the axial depth of cut as shown in Eqs. 7 and 8. The computer code accommodates the entry and exit angles automatically and calculates a positive value for the uncut chip thickness only when the cutters are engaged with the workpiece. Since the axial forces acting on the tool during micro-milling processes are very low compared to tangential and normal forces [22], only forces in the feed and cross-feed direction, namely F_x, F_y are considered in this study.

3 Experimental setup

Slot and side micro-milling tests were conducted on commercially pure titanium (cp-Ti grade 2) on a Mikrotools DT-110 3-axis micro-milling center, equipped with a

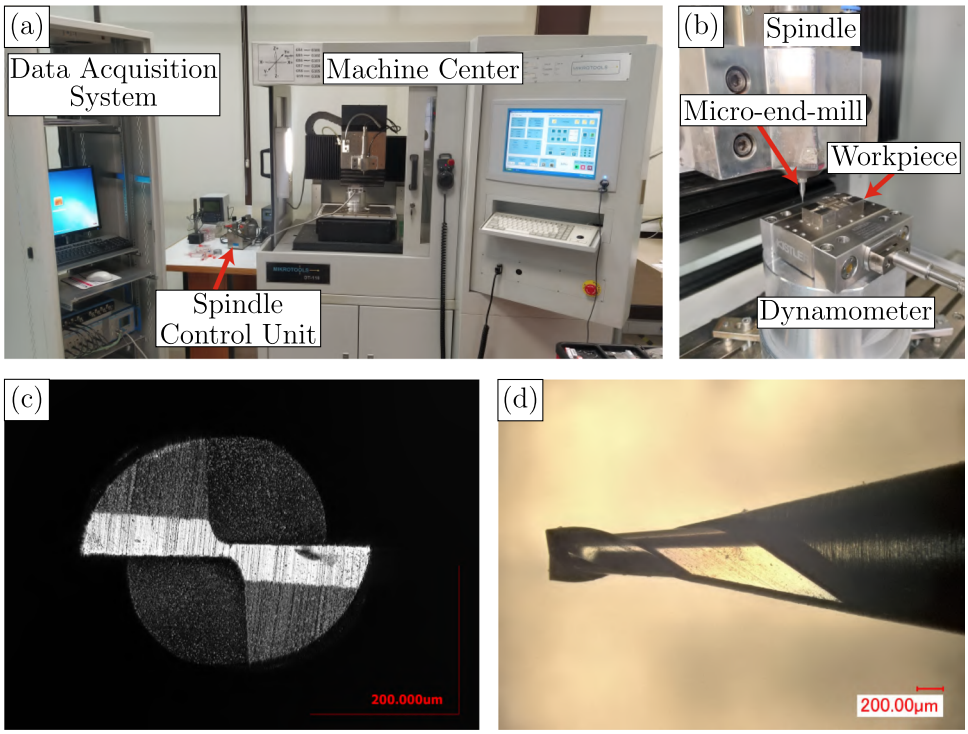

Fig. 10 Experimental setup: (a) CNC micro-machining center and data acquisition system. (b) High speed spindle and dynamometer. (c) Bottom view of the micro-end-mill. (d) Side view of the micro-end-mill

high precision Nakanishi NR40-5100 ATC Automatic Tool Replacement Spindle with EM-3060 Brushless Motor (Fig. 10a–b). A coated carbide two-flute micro-end mill (Fig. 10c–d) with 400-μm diameter, 800-μm length of cut, and 30-degree helix angle (MXH230 0.4×0.8 NS Tools, Japan) was used to machine slots of 10-mm length at a fixed spindle speed of 25,000 rpm and a fixed axial depth of cut of 40 μm. The feed per tooth values used during the experiments were $f_t = 1, 2, 4, 6, 8, 10\mu$m/tooth. The edge radius of the tool (r_e) was measured as 1.78 μm. The cutting forces were measured using a Kistler mini dynamometer 9256C1 connected to a multichannel charge amplifier, at a sampling frequency of 333.3 kHz (3 μs). The forces are stored on a computer in LABView environment. Before investigating the machined surfaces, the workpiece was cleaned using an ultrasonic cleaner. The machined surfaces were scanned using a laser microscope at a 100× objective lens (Keyence VKX 100).

4 Micro-milled surface topography analysis

The machined surfaces are investigated with a laser scanning microscope in order to analyze the feed marks of the cutting teeth of the tool on the workpiece. Surface data from the floors of the slot milling experiments and the side walls of side-milling experiments are analyzed to identify the runout parameters and the value of the minimum uncut chip thickness as shown in Fig. 11. This figure is rendered using the actual laser scans of the machined surfaces as

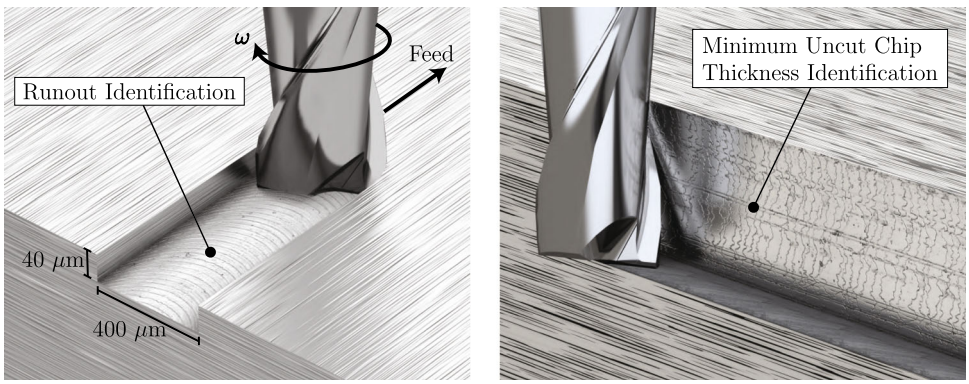

Fig. 11 Machined surface investigation to identify (a) runout parameters and (b) minimum uncut chip thickness

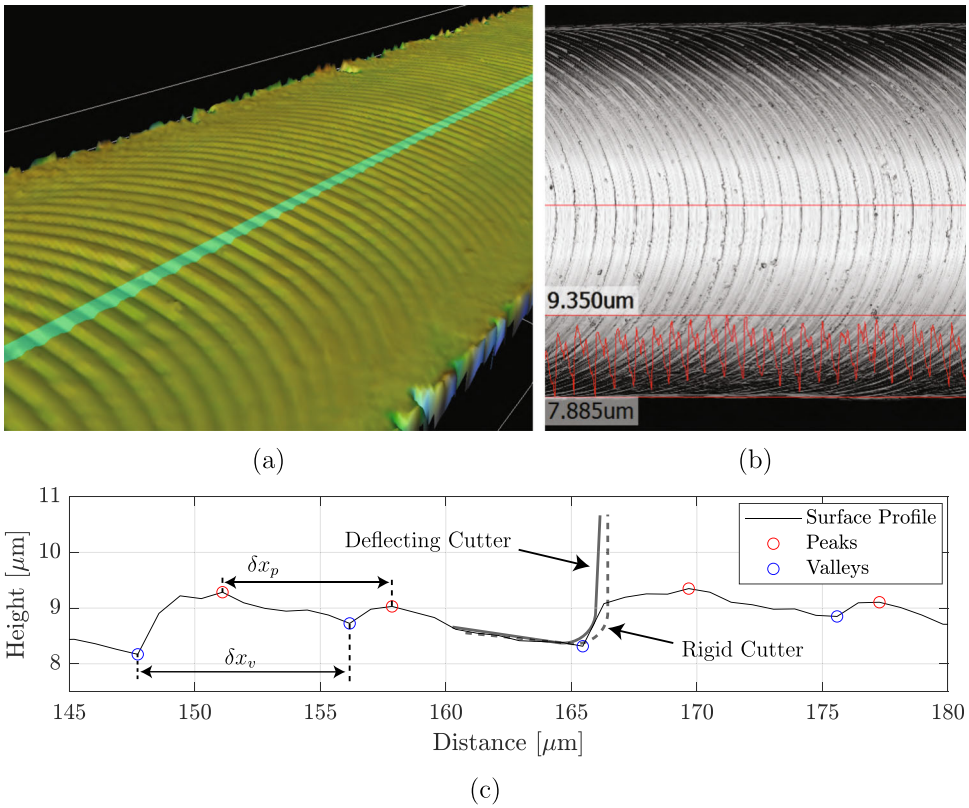

Fig. 12 Machined surface investigation: (a) 3D surface height map. (b) Laser scan of the surface and line profile measurement. (c) Peak analysis of the surface profile measurement (10 μm/tooth)

texture maps in a rendering software (Solidworks Visualize Professional, Dassault Systèmes, France).

4.1 Investigation of machined surface floor

A line profile was taken at the centerline of the slot, which corresponds to the maximum chip thickness and a peak detection algorithm was used to identify the surface profile's peaks and valleys (Fig. 12). It can be noted from Fig. 12c that the depth of valleys is alternating, which may be related to the actual tool geometry and tool deflection in the presence of runout. Tool runout results in a variation in the chip load between the two consequent tooth passes. As a result, the normal force would also vary according to the chip load, which would affect tool deflection. The deeper scratches on the surface can be related to the larger bending of the tool tip, and the depth of these scratches alternates.

The horizontal distances between the peaks δx_p and the valleys δx_v are calculated using a computer code, and they are represented in histograms in Fig. 13.

The histogram in Fig. 13a shows two values averaging near 8 and 12 μm. This is the combined effect of runout parameters on the actual chip thickness at the centerline of the slot, as the commanded feed was 10 μm in this case. The histogram in Fig. 13b shows a normal distribution of around 10 μm. The fact that the alternation is visible on the

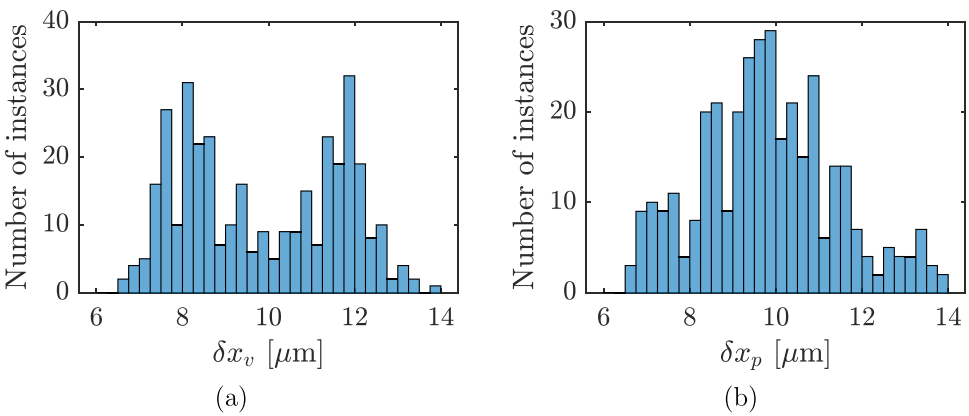

Fig. 13 Histogram distributions of the peak analysis results at 10 μm/tooth feed: (a) Horizontal distance between valleys (δx_v). (b) Horizontal distance between peaks (δx_p)

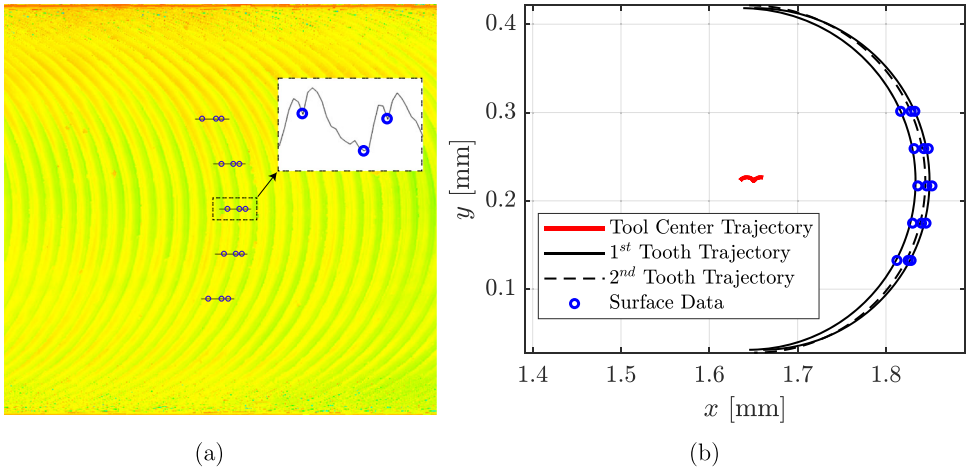

Fig. 14 Surface investigation: (a) Selection of surface data points for optimization at 8 μm/tooth feed. (b) Optimized tooth trajectories at 8 μm/tooth feed

histogram of the valleys but not the peaks can be explained by the likelihood of subsequent tooth passes altering the top of the surface profile but not the bottom. Therefore, it can be assumed that this profile's valleys represent the intersection of the cutting teeth trajectories with the centerline of the slot, and the horizontal distance between these valleys (δx_v) represents the chip thickness at that location. It must be noted that the histogram data does not provide information related to runout angle as it was collected only from the centerline. Multiple solution pairs of runout radius and angle may be found. To identify a single solution, point coordinates belonging to three consecutive tooth passes on the surface were located considering the surface topography and profile valleys, as depicted in Fig. 14. The surface marks were selected carefully such that the resulting values of δx_v at the centerline correspond to the most occurring values indicated from the histogram distributions. They are then used with a modified trajectory equation in an optimization algorithm to isolate a single solution.

The uncut chip thickness model that was developed in Section 2 is utilized to identify runout radius and angle parameters. First, the absolute error between the averages of experimental and simulated maximum uncut chip thickness resulting from the two different cutting teeth of the micro-end-mill at 6,8,10 feeds is minimized by optimization of the following fitness function using the genetic algorithm as shown in Eq. 26. The algorithm is set to halt when the average change in the fitness function value throughout 20 stall generations is less than a predefined tolerance of 10^{-6}.

$$\varepsilon = \sum_{f_t=6,8,10} \sum_{j=0,1} \left| \overline{h_{rd}}|_{\max} \left(\theta_{\frac{K}{2},j}\right)_{\exp} - \overline{h_{rd}}|_{\max} \left(\theta_{\frac{K}{2},j}\right)_{\text{sim}} \right| \quad (26)$$

A genetic algorithm was used again to minimize the summation of the shortest distances from each data point on the three subsequent tooth passes to the corresponding simulated tooth trajectories that are calculated using a modified expression of Eq. 10a as follows:

$$x_P(t_1) = x_o + x_C(t_1) + R\sin\left(\omega t_1 - \frac{2\pi j}{N_z}\right) \quad (27a)$$

$$y_P(t_1) = y_o + y_C(t_1) + R\cos\left(\omega t_1 - \frac{2\pi j}{N_z}\right) \quad (27b)$$

where x_o, y_o are offset parameters that are included in the optimization algorithm in order to find the location of the origin of the reference plane in which the tooth trajectories are simulated.

The solutions obtained from the optimization algorithm using a single location (centerline of the slot) were plotted against each other as shown in Fig. 15. It was observed from the figure that the runout parameters are co-dependent. The fitness function values ranged from 3.04×10^{-3} to 3.06×10^{-3}, which gives a difference of only ~0.8% between the

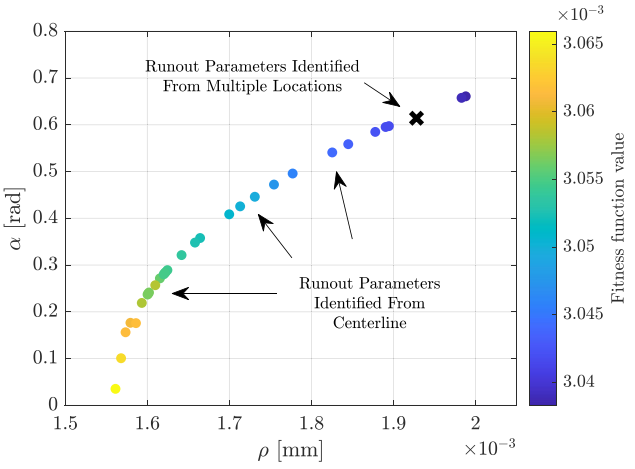

Fig. 15 Runout parameter optimization results

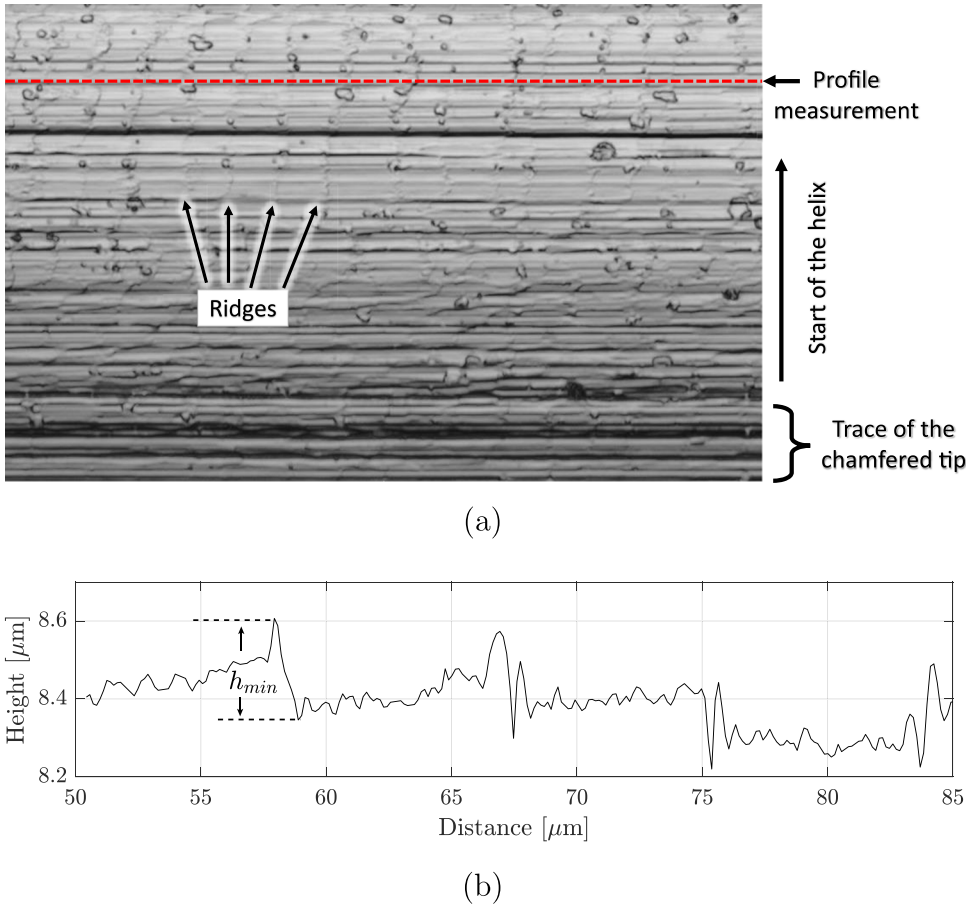

Fig. 16 Investigation of the side walls. (a) Surface topography. (b) Surface profile measurement and identification of the minimum uncut chip thickness

best and worst solutions. The runout solutions obtained by analysis of the machined surface at the centerline of the slot floor were used in the cutting force model to look at the error in the force predictions. The error was calculated as the summation of the RMS errors in the force signal in both the x and y directions. The error ranged from 0.3775 to 0.381, which gives a difference of only (∼0.91%) in total RMS error between the best and worst solutions. The single solution yielded from the optimization algorithm using the surface marks of three consecutive tooth passes is marked with an "x" in Fig. 15.

It is important to note that the scanned surfaces are the elastically recovered after machining. Therefore, the effect of elastic recovery is already included in the identified runout parameters. The elastic recovery ratio depends on the chip thickness and it is unknown. It has been shown in a previous study that the effect of elastic recovery is more significant at lower feed rates [32]. Therefore, the surface investigation to identify the runout parameters was carried out at a relatively high feed rate in this study (i.e., 6,8,10 μm/tooth), where tool deflection would also be more influential.

4.2 Identification of minimum uncut chip thickness

The minimum uncut chip thickness was measured experimentally by investigating the side walls of the milled surface (Fig. 16). The measurement of the ridges that were left on the surface indicates transitions between ploughing and cutting, as suggested by Liu et al. [6]. A set of five side milling

Table 1 Side milling conditions

Test number	Axial depth of cut	Radial depth of cut	Radial immersion (%)
1	100 μm	100 μm	25%
2	100 μm	150 μm	37.5%
3	100 μm	180 μm	45%
4	150 μm	180 μm	45%
5	150 μm	150 μm	37.5%

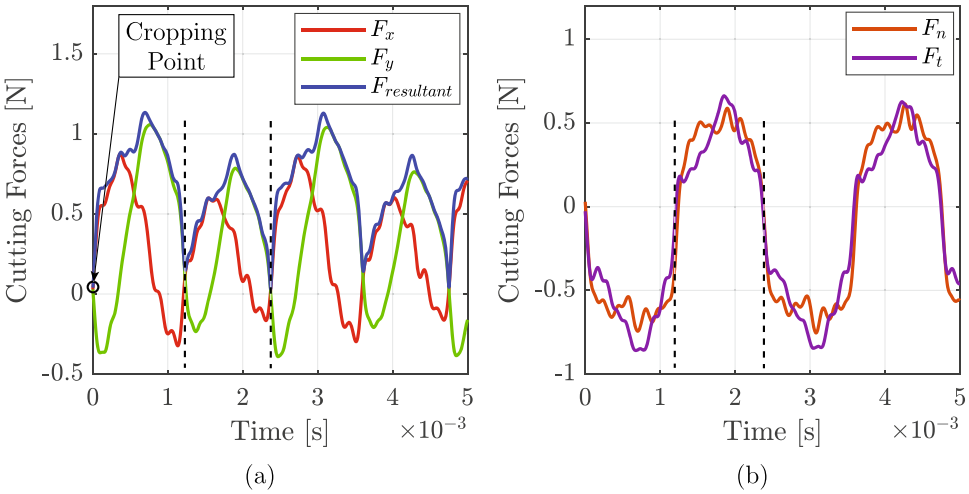

Fig. 17 Experimental cutting force signal (at 2 μm/tooth feed). (a) Signal in the workpiece reference plane. (b) Signal in the tool rotating reference plane

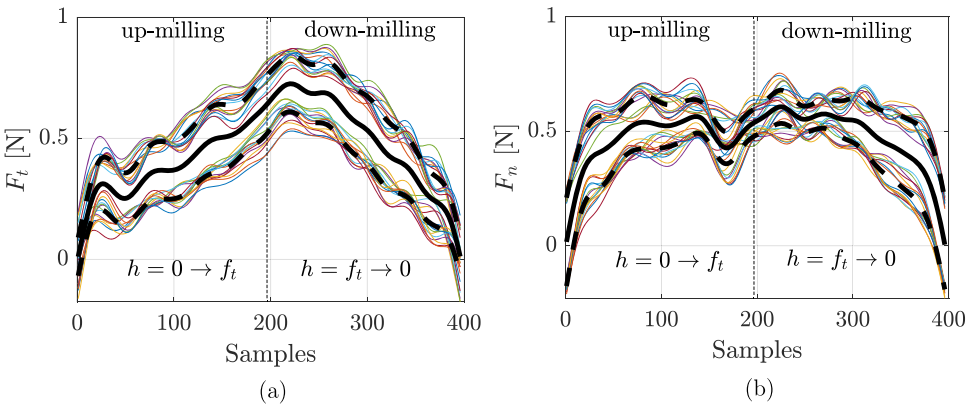

Fig. 18 Splitting and averaging the force signal. (a) Tangential force. (b) Normal force

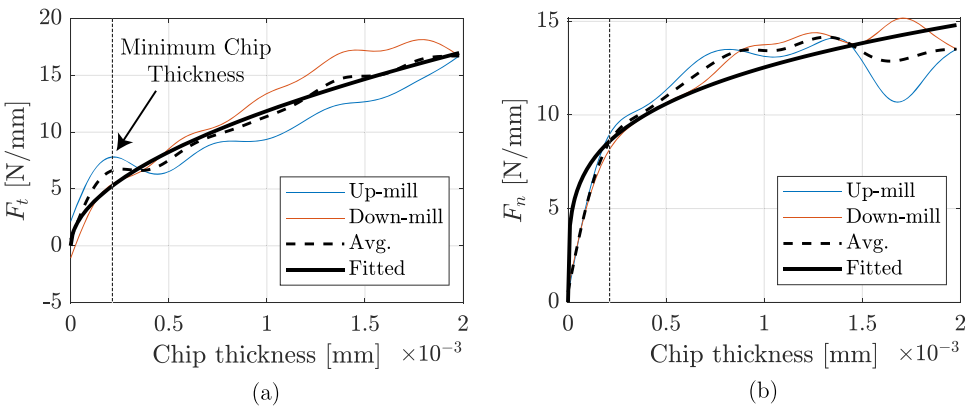

Fig. 19 Curve fitting the force signal. (a) Tangential force. (b) Normal force

tests were conducted using the same tool and workpiece, while keeping the spindle speed constant at 25000 rpm, the feed constant at 4 μm, and varying the axial and radial depth of cut as shown in Table 1. The cutting length of the tests was 2 mm. The side wall surfaces were scanned with the laser scanning microscope using a 50× objective lens, and horizontal profile measurements were taken at three different heights at 25-μm increments on the side walls.

The average value considering all the profile measurements for the five cutting tests was calculated as 0.2 μm, and it was assumed as the minimum uncut chip thickness value. The edge radius of the tool (r_e) was measured as 1.78 μm, which gives a $h_{\min}/r_e$ ratio of 0.11 (11%) for the tool and work material pair considered in this study.

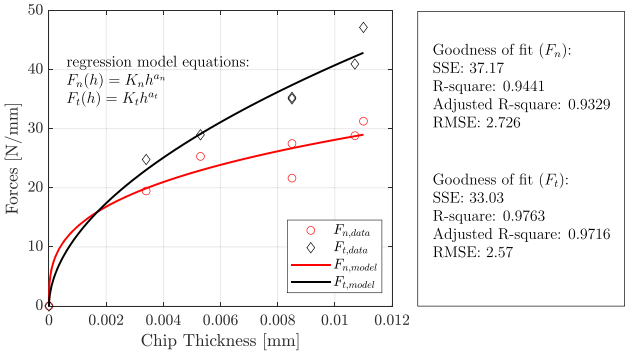

Fig. 20 Curve fitting of the chip/force data pairs and identification of the cutting coefficients

5 Force signal processing and identification of the cutting force coefficients

The measured force signal during slot milling tests was processed with a low-pass filter applied at a frequency of 3300 Hz to filter out higher-order harmonics. A fast Fourier transformation was used to identify the actual spindle speed by investigating the frequency content of the measured force signal. The actual spindle speed was found to be 25,252 rpm. The signal's frequency content was also investigated for chatter, which was not present. The resultant force signal was calculated, and peak analysis was carried out to identify the signal valleys. The signals were cropped at a valley point as shown in Fig. 17, which was chosen as the starting time t_o. The cutting force signal was then transformed to the rotating reference plane of the tool (F_t, F_n) using an inverse of the transformation presented in Eq. 7.

To identify the ploughing coefficients, the slot milling force signal in the rotating reference plane of the tool was split into equal segments representing one tooth pass each, with separate consideration of the two cutting teeth of the tool. The resultant force signal valleys were used to quantify the segments. The signal segments for the second cutting tooth were flipped. Then, all the segments are plotted on top of each other and averaged, as shown in Fig. 18. The effect of runout is obvious on the averaged signals as the averaged curves representing the first and second cutting teeth alternate in magnitude (black dashed curves in Fig. 18). A final average was taken for both dotted curves (solid black curve in Fig. 18). It was assumed that the chip thickness reaches a maximum value at $\theta = \pi/2$. Since the curves were averaged for both cutting teeth of the tool, this value should correspond to the feed per tooth value f_t. Using this assumption, the up-milling and down-milling segments of the final curve are averaged and normalized by the axial depth of cut. Then a power law equation was fit to the data by minimization of the least squared error (Fig. 19), thus identifying the ploughing coefficients. The effect of the minimum chip thickness can be observed on the tangential force in Fig. 19a, where a sudden change in the slope of the up-milling force signal implies a transition from ploughing to cutting action. The value of the assumed chip thickness in this region agrees with the value of the minimum uncut chip thickness identified in Section 4.2.

To identify the force coefficients in the cutting dominated regions, peak analysis was carried out to identify the peaks of the experimental normal and tangential forces. Based on the surface analysis carried out in Section 4, the peak values of the normal and tangential forces were linked to the maximum chip thickness, which was extracted from the centerline of the slot floor at three different feeds: 6, 8, and 10 μm/tooth. Weighted averages of three histogram bins (Fig. 13a) were taken to identify two maximum chip thickness values corresponding to the two different cutting edges of the tool at each of the aforementioned feeds.

Table 2 Identified model parameters

	Ploughing		Cutting	
Force coefficients	K_{np} (N/mm^2)	a_{np}	K_{nc} (N/mm^2)	a_{nc}
	79.64	0.2577	122.8	0.32
	K_{tp} (N/mm^2)	a_{tp}	K_{tc} (N/mm^2)	a_{tc}
	526.7	0.5670	465.4	0.5288
Runout parameters	ρ		α	
	1.82 μm		0.58 rad	

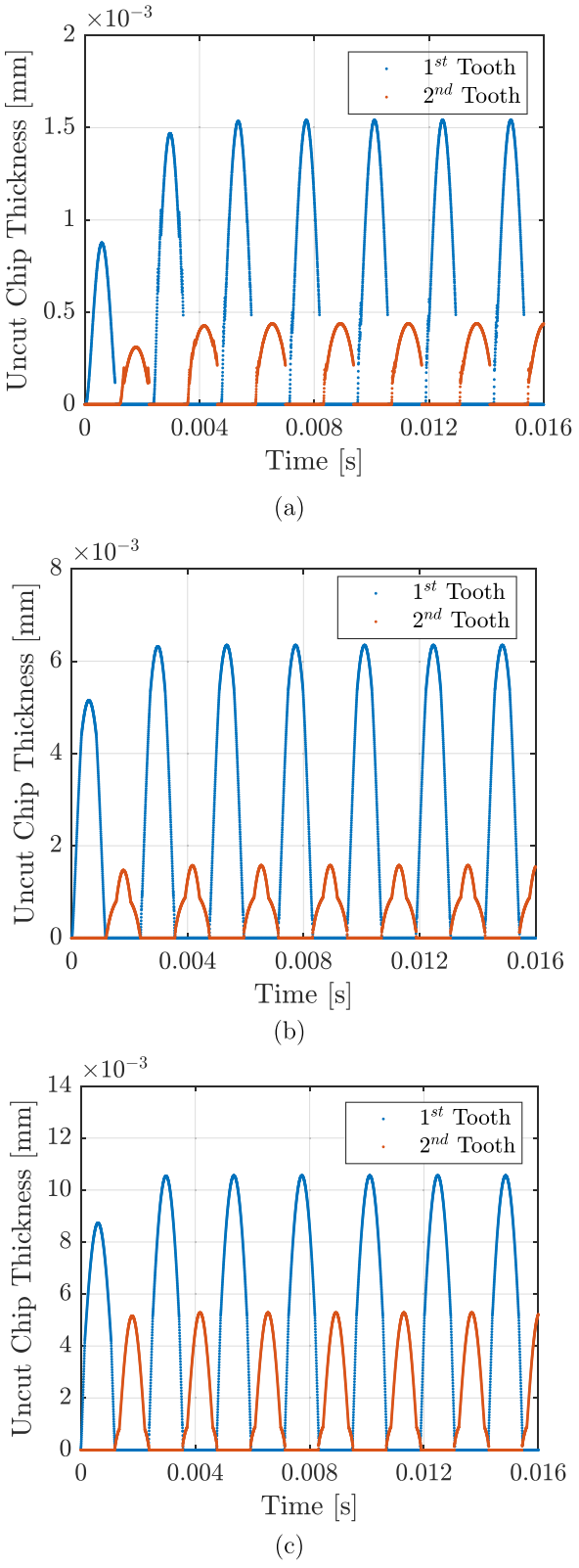

Fig. 21 Simulated uncut chip thickness at (a) 1 μm/tooth, (b) 4 μm/tooth, and (c) 8 μm/tooth

The resulting force/chip data pairs are plotted as shown in Fig. 20, and two power law functions for the normal and tangential forces are used in a curve fitting algorithm to fit the experimental data, thus identifying the cutting coefficients. The identified force coefficients and runout parameters are presented in Table 2.

6 Results and discussion

Figure 21 shows the simulated uncut chip thickness at three different feed per tooth values, namely 1, 4, and 8 μm/tooth. Figure 22 shows the predicted cutting force signal compared to the measured data at the same feed values. The root mean squared error between the predicted and measured cutting force signal is reported in Table 3. The cutting force model produces accurate predictions of the force measurements over a wide range of feed values, as seen in Fig. 22 and Table 3. Predictions of the cutting forces near the entry and exit of the cut are shown to be in good agreement with experimental data.

Side milling simulations were also carried out to evaluate the model performance in low radial immersion operations. As mentioned in Section 2, the model is able to identify the entry and exit angles and produce positive chip thickness values when the cutting teeth are engaged with the workpiece material in the case of slot milling. In the case of side milling, the entry and exit angles are calculated as following:

$$\theta_{en} = \begin{cases} 0 & \text{up-milling} \\ \pi - \cos^{-1}\left(\frac{R-a_e}{R}\right) & \text{down-milling} \end{cases} \tag{28a}$$

$$\theta_{ex} = \begin{cases} \cos^{-1}\left(\frac{R-a_e}{R}\right) & \text{up-milling} \\ \pi & \text{down-milling} \end{cases} \tag{28b}$$

where θ_{en}, θ_{ex} are the entry and exit angles in radians, and a_e is the radial depth of cut in mm. Figures 23 and 24 show the simulation results for the side milling tests no. 1 and 5 (see Table 1). The figures show also good agreement between the experimental and simulated cutting force signal in low immersion conditions.

The root mean squared error between the predicted and measured cutting force signal is reported in Table 4. The cutting force model produces accurate predictions of the force measurements or the two different cases, as seen in Fig. 24 and Table 4. Predictions of the cutting forces near the entry and exit of the cut are shown to be in good agreement with experimental data.

In order to investigate the influence of different runout parameters on the process outputs, the same end mill was

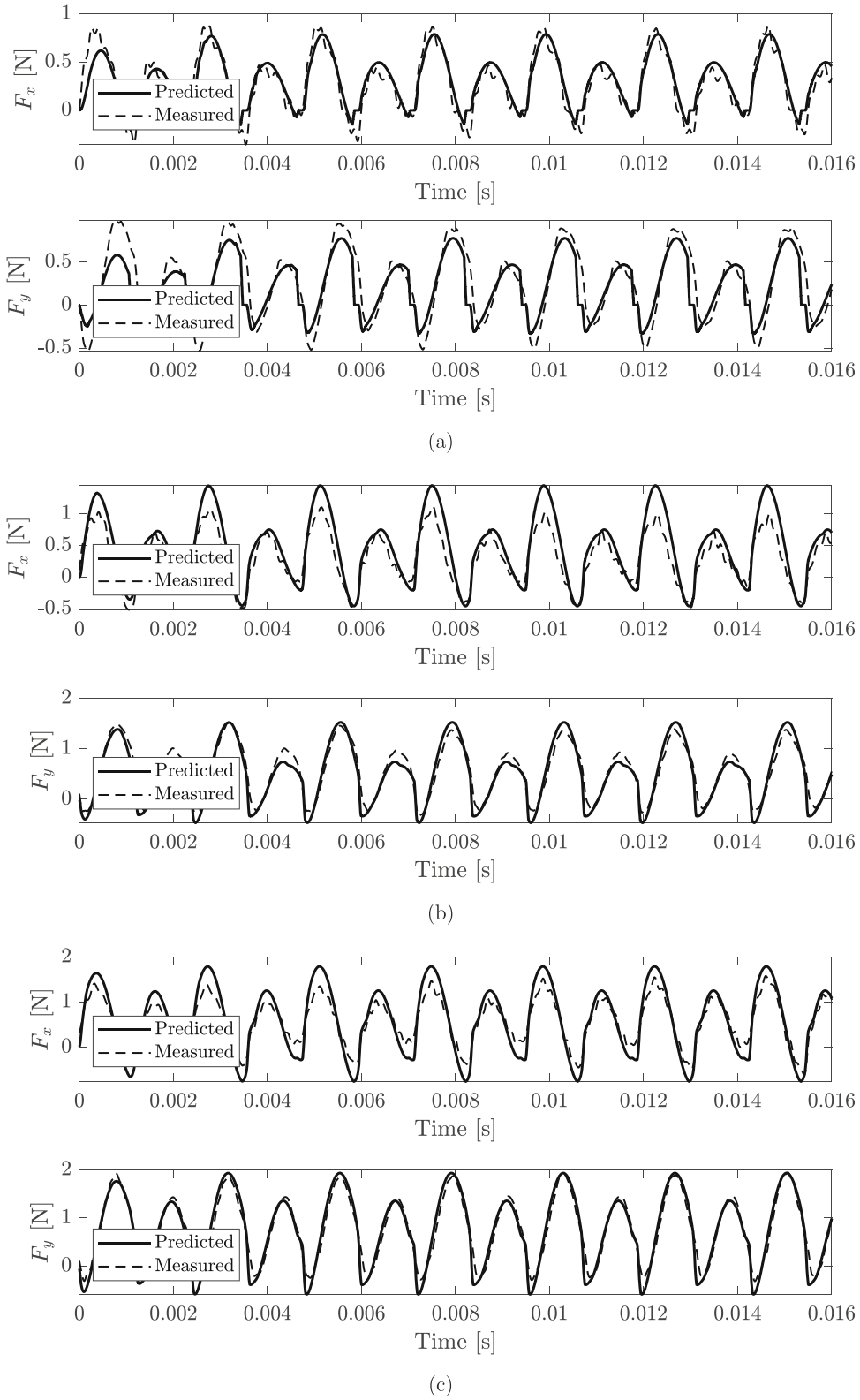

Fig. 22 Simulated and measured cutting force signal at (a) 1 μm/tooth, (b) 4 μm/tooth, and (c) 8 μm/tooth

removed and re-clamped on the spindle in a different orientation (runout condition 2). All the experimental conditions were held constant, and the analysis presented in Section 4.1 was carried out again.

The solutions for the first and second runout conditions are presented in Fig. 25. In both cases, force predictions with similar order of accuracy were obtained for all the solutions per runout condition. The same trend was

Table 3 RMS error in the cutting force signal for slot milling tests

Feed	RMSE in F_x	RMSE in F_y
1 μm/tooth	0.0346	0.0376
4 μm/tooth	0.1609	0.0492
8 μm/tooth	0.0273	0.0081

observed; however, the solutions were spread over a broader curve, indicating a different runout condition. In this case, the runout radius and the runout angle were identified as 1.74 μm and 0.88 rad, respectively.

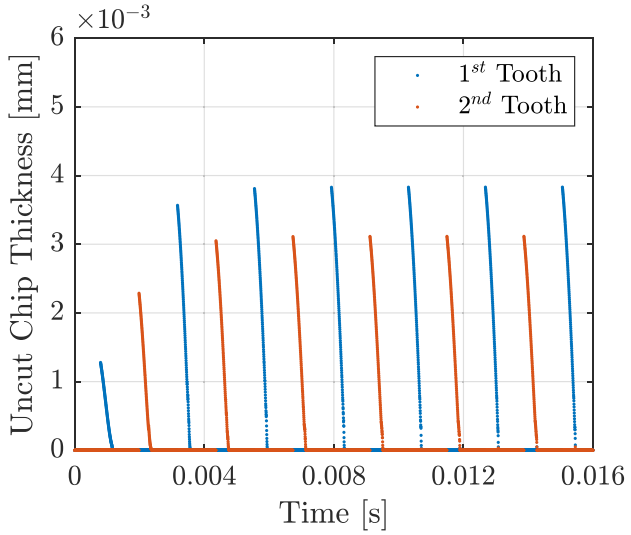

Fig. 23 Simulated uncut chip thickness during side milling: (a) Test no. 1. (b) Test no. 5

Figure 26 compares the simulated and measured forces in the second runout condition. Accurate predictions were also obtained in this case, as seen in the figure. The peak and RMS values of the resultant force signal for both runout conditions were calculated and plotted against the feed, as shown in Fig. 27. The trends in forces are observed to be quite close.

The areal surface roughness was investigated under the laser scanning microscope for both cases. The areal surface roughness measurements are plotted against the feed per tooth values for both runout conditions, as shown in Fig. 28. It can be observed that the surface quality at the lower feed values is poor, which is expected due to the dominance of ploughing action. The surface quality improves as the feed per tooth is increased until the best surface quality (Fig. 29) is achieved at a feed of 4 μm. The surface quality starts to worsen again as the feed per tooth is increased, which can be related to higher cutting forces that are associated with tool deflection. The surface roughness trend in both runout conditions appears similar. However, surface quality appears to be worse at higher feeds in runout condition 1, as the runout was more severe in that case.

7 Conclusion

A micro-milling force model which utilizes machined surface topography information is presented in this study. The variation of uncut chip thickness depending on the effect of helix lag and trochoidal trajectories of all the previous passes of micro-end-mill teeth with consideration of runout, tool deflection, and chip thickness accumulation is included in the model. The runout parameters are extracted from the surface marks of the machined surface using peak analysis and optimization of the uncut chip thickness model. The following conclusions can be drawn from this work:

- The proposed runout calibration method using the machined surface topography was successfully used to identify runout conditions during micro-milling of commercially pure titanium.
- The effect of runout is observed on the histograms of the horizontal valley-to-valley distances. This was explained by the fact that subsequent tooth passes can alter the top of the machined surface, but not the bottom. The valley data was related to the actual chip thickness and was used to extract runout parameters.
- It is shown that the runout radius and runout angle are codependent in force modeling of micro-milling, and that multiple pairs of runout parameters can be used to produce force predictions in the same order of accuracy. Using optimization, a single solution of

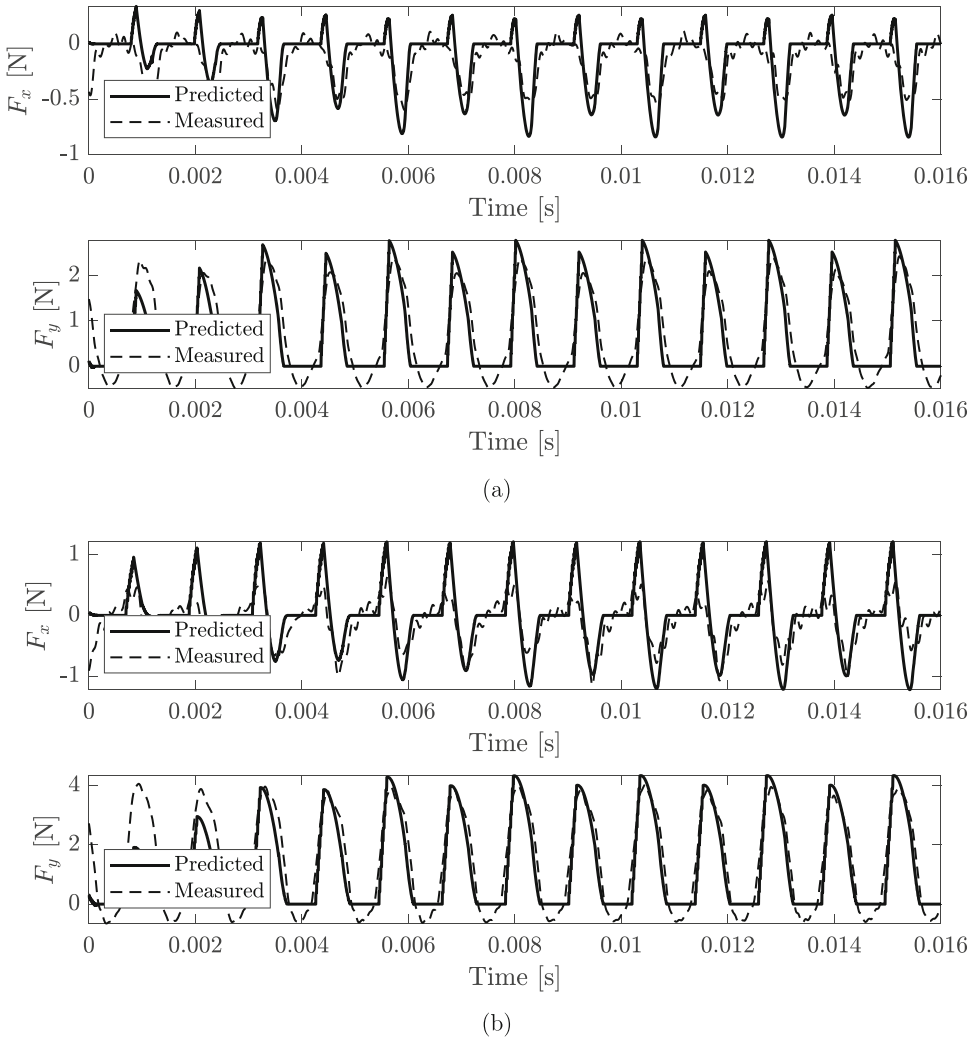

Fig. 24 Simulated and measured cutting force signals during side milling: (a) Test no. 1. (b) Test no. 5

the runout parameters was identified by fitting the simulated cutting tooth trajectories to the feed marks on the actual machined surface.

- The minimum uncut chip thickness value was identified from the side walls during side milling of cpTi, and the minimum uncut chip thickness to edge radius ratio ($h_{\min}/r_e$) was found to be 11% in this study.
- If axial and radial run-out parameters can be measured dynamically with non-contact methods, the approach proposed here can be used to predict surface topography. The proposed model can be further extended to identify elastic recovery rate of the material.

Table 4 RMS error in the cutting force signal for side milling tests

Test number	RMSE in F_x	RMSE in F_y
1	0.0275	0.0225
5	0.0941	0.1057

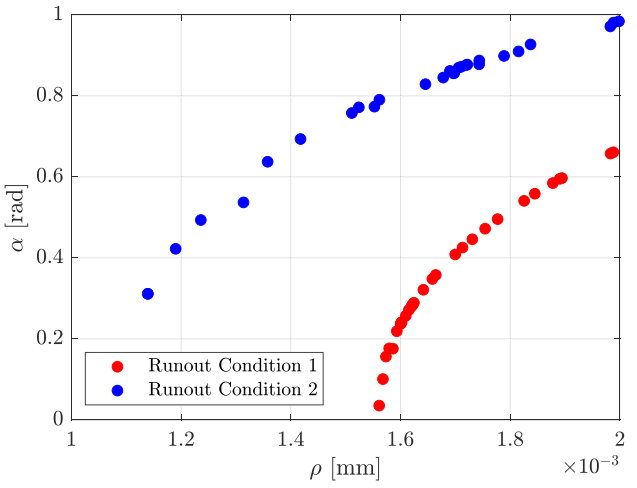

Fig. 25 Runout parameter optimization results for both runout conditions

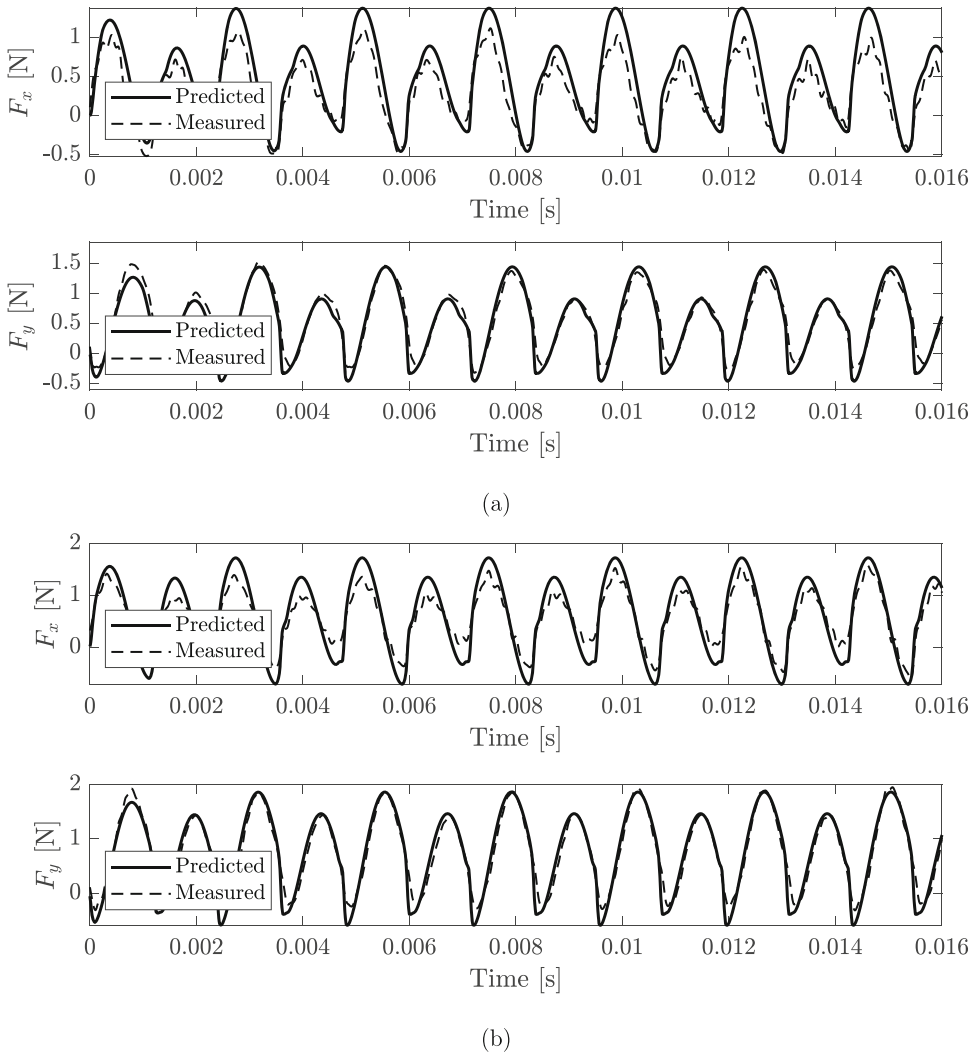

Fig. 26 Simulated and measured cutting force signal in the second runout condition at (a) 4 μm/tooth and (b) 8 μm/tooth

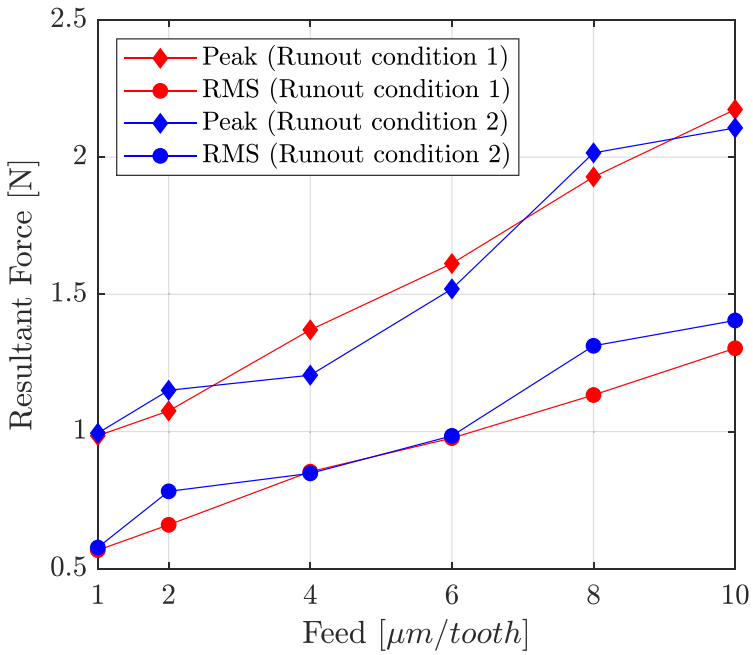

Fig. 27 Peak and RMS values of the resultant force signal vs. feed for both runout conditions

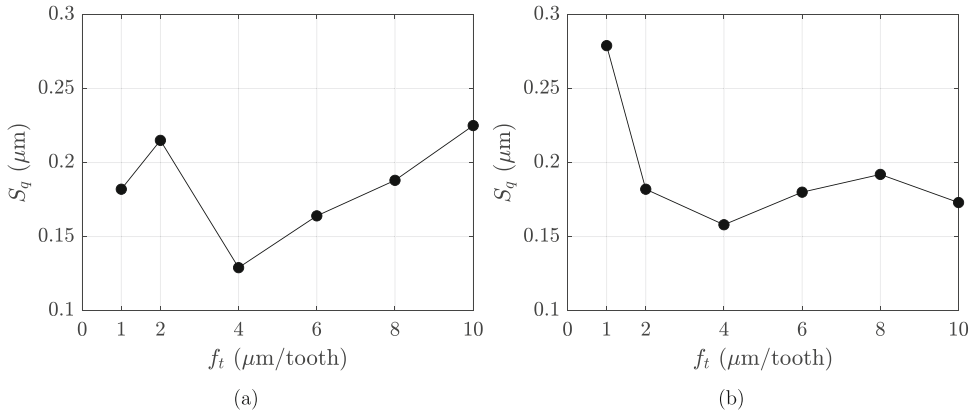

Fig. 28 Surface roughness vs. feed values. (a) Runout condition 1. (b) Runout condition 2

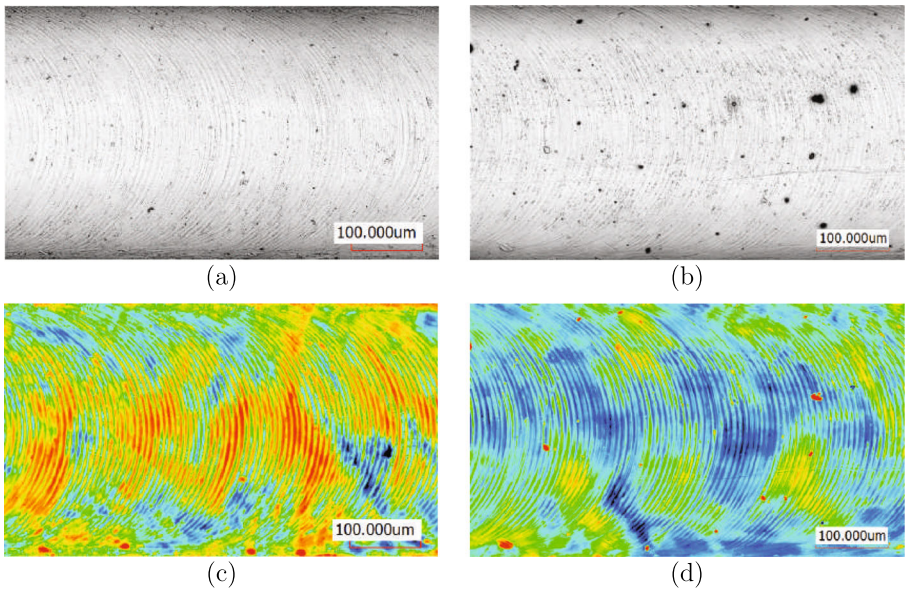

Fig. 29 Topography of the best surface (at 4 µm/tooth). (a), (c) Runout condition 1. (a), (d) Runout condition 2

Author Contributions Abdulrzak Masrani: writing, measurement, data analysis, conceptualization, methodology, software; Yigit Karpat: conceptualization, methodology, supervision.

Data Availability The data may be available if requested from the corresponding author.

Code availability The code is not available.

Declarations

Ethics approval Not applicable.

Consent to participate Not applicable.

Consent for publication Not applicable.

Competing interests The authors declare no competing interests.

References

1. Serje D, Pacheco J, Diez E (2020) Micromilling research: current trends and future prospects. The International Journal of Advanced Manufacturing Technology 111(7):1889–1916
2. O'Toole L, Kang C-W, Fang F-Z (2021) Precision micro-milling process: state of the art. Advances in Manufacturing 9(2):173–205
3. Chen N, Li HN, Wu J, Li Z, Li L, Liu G, He N (2021) Advances in micro milling: from tool fabrication to process outcomes. Int J Mach Tools Manuf 160:103670
4. Kim C-J, Mayor JR, Ni J (2005) A static model of chip formation in microscale milling. J Manuf Sci Eng 126(4):710–718
5. de Oliveira FB, Rodrigues AR, Coelho RT, de Souza AF (2015) Size effect and minimum chip thickness in micromilling. Int J Mach Tools Manuf 89:39–54
6. Liu X, DeVor RE, Kapoor SG (2005) An analytical model for the prediction of minimum chip thickness in micromachining. J Manuf Sci Eng 128(2):474–481
7. Rezaei H, Sadeghi MH, Budak E (2018) Determination of minimum uncut chip thickness under various machining conditions during micro-milling of Ti-6Al-4V. The International Journal of Advanced Manufacturing Technology 95(5):1617–1634

8. Bao W, Tansel I (2000) Modeling micro-end-milling operations. part ii: tool run-out. Int J Mach Tools Manuf 40(15):2175–2192
9. Li C, Lai X, Li H, Ni J (2007) Modeling of three-dimensional cutting forces in micro-end-milling. J Micromech Microeng 17(4):671–678
10. Mamedov A, Lazoglu I (2016) An evaluation of micro milling chip thickness models for the process mechanics. The International Journal of Advanced Manufacturing Technology 87(5):1843–1849
11. Afazov S, Zdebski D, Ratchev S, Segal J, Liu S (2013) Effects of micro-milling conditions on the cutting forces and process stability. J Mater Process Technol 213(5):671–684
12. Malekian M, Mostofa M, Park S, Jun M (2012) Modeling of minimum uncut chip thickness in micro machining of aluminum. J Mater Process Technol 212(3):553–559. Micro-Manufacturing Processes
13. Zhang X, Wang X, Zhao Z, Chen K, Yin J, Zhao W (2022) A general on-machine non-contact calibration method for milling cutter runout. The International Journal of Advanced Manufacturing Technology 120:7341–7361
14. Jing X, Lv R, Song B, Xu J, Jaffery SHI, Li H (2021) A novel run-out model based on spatial tool position for micro-milling force prediction. J Manuf Process 68:739–749
15. Wang W, Zhang W, Huang D, Wang W (2021) Cutting force modeling and experimental validation for micro end milling. The International Journal of Advanced Manufacturing Technology 117(3):933–947
16. Attanasio A (2017) Tool run-out measurement in micro milling. Micromachines, vol 8(7)
17. Oliaei SNB, Karpat Y (2016) Influence of tool wear on machining forces and tool deflections during micro milling. The International Journal of Advanced Manufacturing Technology 84(9):1963–1980
18. Rodríguez P, Labarga JE (2015) Tool deflection model for micromilling processes. The International Journal of Advanced Manufacturing Technology 76(1):199–207
19. Mamedov A, S.E.L. K, Lazoglu I (2015) Instantaneous tool deflection model for micro milling. The International Journal of Advanced Manufacturing Technology 79:769–777
20. Moges TM, Desai KA, Rao PVM (2018) Modeling of cutting force, tool deflection, and surface error in micro-milling operation. The International Journal of Advanced Manufacturing Technology 98(9):2865–2881
21. Malekian M, Park SS, Jun MB (2009) Modeling of dynamic micro-milling cutting forces. Int J Mach Tools Manuf 49(7):586–598
22. Zhang X, Ehmann KF, Yu T, Wang W (2016) Cutting forces in micro-end-milling processes. Int J Mach Tools Manuf 107:21–40
23. Zhou Y, Tian Y, Jing X, Ehmann KF (2017) A novel instantaneous uncut chip thickness model for mechanistic cutting force model in micro-end-milling. The International Journal of Advanced Manufacturing Technology 93(5):2305–2319
24. Jin X, Altintas Y (2012) Prediction of micro-milling forces with finite element method. J Mater Process Technol 212(3):542–552. Micro-Manufacturing Processes
25. Wojciechowski S, Matuszak M, Powałka B, Madajewski M, Maruda R, Królczyk G (2019) Prediction of cutting forces during micro end milling considering chip thickness accumulation. Int J Mach Tools Manuf 147:103466
26. Sahoo P, Patra K, Singh VK, Mittal RK, Singh RK (2020) Modeling dynamic stability and cutting forces in micro milling of Ti6Al4V using intermittent oblique cutting finite element method simulation-based force coefficients. J Manuf Sci Eng 142(9):091005
27. Jing X, Li H, Wang J, Tian Y (2014) Modelling the cutting forces in micro-end-milling using a hybrid approach. The International Journal of Advanced Manufacturing Technology 73(9):1647–1656
28. Attanasio A, Abeni A, Özel T, Ceretti E (2019) Finite element simulation of high speed micro milling in the presence of tool run-out with experimental validations. The International Journal of Advanced Manufacturing Technology 100(1):25–35
29. Vogler MP, DeVor RE, Kapoor SG (2005) On the modeling and analysis of machining performance in Micro-Endmilling, part i: surface generation. J Manuf Sci Eng 126(4):685–694
30. Krüger M, Denkena B (2013) Model-based identification of tool runout in end milling and estimation of surface roughness from measured cutting forces. The International Journal of Advanced Manufacturing Technology 65(5):1067–1080
31. Chen W, Sun Y, Huo D, Teng X (2019) Modelling of the influence of tool runout on surface generation in micro milling. Chinese Journal of Mechanical Engineering 32(1):2
32. Jing X, Song B, Xu J, Zhang D (2022) Mathematical modeling and experimental verification of surface roughness in micro-end-milling. The International Journal of Advanced Manufacturing Technology 120:7627–7637
33. Gilat A (2013) Numerical methods for engineers and scientists Wiley Global Education
34. Mamedov A, Layegh SK, Lazoglu I (2013) Machining forces and tool deflections in micro milling, Procedia CIRP, vol 8, pp 147–151 . 14th CIRP Conference on Modeling of Machining Operations (CIRP CMMO)